Third particle ejection effects on wear with quenched and tempered steel fretting contact

Jouko Hintikka [a,*], Arto Lehtovaara [a], Antti Mäntylä [b]

* Corresponding author: Phone: +358 3 311511, Email: jouko.hintikka@tut.fi

[a] Department of Materials Science, Tampere University of Technology

PO Box 589, 33101 Tampere, Finland

[b] Research & Development, Wärtsilä Finland Oy,

PO Box 244, 65101 Vaasa, Finland

ABSTRACT

The design and life prediction of fretting wear sensitive mechanical components remains a challenge. In the present work the role of wear particle movements under conditions of axisymmetric loading of an annular, flat-on-flat contact were investigated using self-mated quenched and tempered steel specimens. Total fretting wear significantly increased when loose wear particles were periodically removed from the interface, and this effect increased as a function of the sliding amplitude. Additionally, increased wear was measured when grooves perpendicular to the sliding direction were added to the interface. Increasing the rate of wear debris ejection leads to increased wear rate because naturally occurring, entrapped third body particles significantly reduce the wear. The shape of fretting loops and values of the average and the maximum coefficient of friction remained unaffected by the removal of entrapped wear debris and by the introduction of the grooves.

Keywords: fretting; unlubricated wear; unlubricated friction; wear debris; third body

INTRODUCTION

Fretting stands for reciprocating surface sliding and wear damage associated with it. Fretting wear and especially fretting fatigue are considered a severe damage mechanism. Fretting damage can accumulate out of sight inside an interface and potentially lead to an unexpected and catastrophic component failure. On steel surfaces, fretting can be detected by the appearance of reddish-brown oxidised wear debris of powdery texture, though such observation requires opening the contact. Design against fretting is made difficult by the fact that there are major uncertainties in the friction and wear behaviour of contacts under a fretting load. (Waterhouse (1) and Hills et al (2))

The motion between contacting first bodies is accommodated via various mechanisms in the interface (i.e., shear and rolling) and further velocity accommodation is enabled by loose and sticking wear debris beds (Berthier et al (3), Berthier (4) and Godet (5,6)). Velocity accommodation via oxide wear particle layers is especially important in fretting conditions because sliding amplitudes are low, and because wear particles tend to get entrapped in the interface (Berthier et al (7)). In such conditions, wear is dictated by the rate of the ejection rather than generation of wear particles. Velocity accommodation in third particles has been studied further in powder lubrication (Iordanoff et al (8), Heshmat (9) and Haff (10)). Because powders have lubricating properties, they can be used to control wear and friction. They provide lift under sliding conditions and retain a load carrying capacity even in static conditions, which may be crucial in fretting.

The role of entrapped wear debris on fretting wear using a flat-on-flat steel contact has been studied, including “open and shut” tests, in which the interface was periodically opened and cleaned of wear debris and in which artificial oxide particles were added in the contact (Colombié et al (11)). They showed that naturally occurring and artificially added beds of oxide particles reduce wear in the first bodies, because the powdery third body has a load carrying capacity that separates the first bodies and accommodated velocity. Fretting wear studies with different radii spheres against flat (Merhej et al (12)) and cylinder against flat (Warmuth et al (13)) have showed that the wear rate reduced when the contact size was increased. These fretting wear observations were explained by the wear reducing properties of the entrapped wear particles, which are more pronounced with larger contacts. Fretting experiments with quenched and tempered steel with large axisymmetrically loaded, annular, flat-on-flat contacts showed wear depending mostly on the sliding amplitude while a normal force had only a slight effect (Hintikka et al (14)). This was also explained by the entrapment of wear particles in the interface, which was assumed especially pronounced due to the large annular contact without any contact edges in the direction of the fretting movement. Furthermore, because pores in the interface affect the accumulation of wear particles in it…

Nomenclature

Symbol	*Explanation*
At-%	Percentage of atoms
COF	Coefficient of friction
COF_{Ed}	Average COF
COF_T	Maximum COF
E	Modulus of elasticity
Ed	Frictional energy dissipation
k	Specimen compliance
N_{Cle}	Number of contact cleanings
$p(r,j)$	Normal pressure distribution
p_n	Nominal normal pressure
P	Normal force at specimen
P_{tot}	Total normal force
r	Radius
r_a	Average radius (10 mm)
r_i	Inner radius (7.5 mm)
r_o	Outer radius (12.5 mm)
S_a	3D average surface roughness
S_u	Ultimate stress
S_y	Yield stress (0.2 %)
S_q	3D root mean squared roughness
S_z	3D max peak to valley distance
W_{Cle}	Mass loss due to contact cleaning
W_{LC}	Mass loss due to load cycles
W_{tot}	Total mass loss
T	Torque
u	Sliding
u_a	Sliding amplitude
x,y,z	Coordinate system
j	Angle around specimen
q	Rotation
q_a	Rotation amplitude
q_k	Corrected rotation
n	Poisson's ratio
Abbr.	
Cle	Contact cleaning tests
EDS	Energy dispersive X-ray spectroscopy
Gro_6	Tests with grooved specimens
Gro_{12}	(6 and 12 grooves)
SEM	Scanning electron microscope
Sta	Tests with standard specimens

…(Varenberg et al (15)), surface topography such as surface roughness contributes to the entrapment of these particles.

The propagation of wear damage may not be linear as a function of the loading parameters, and transitions may occur in wear rate (Blau (16)). Calculating the wear rate from pre- and post-test measurements may be misleading if the running-in or wear-in effects are pronounced. Changes in wear rate occur also in fretting wear, where wear may initially be adhesive and then gradually change to abrasive due to entrapped wear particles (Colombié et al (11) and Hintikka et al (14)).

The rate of fretting wear has been shown to depend on loose wear particles entrapped in the contact; therefore, modifying the conditions of entrapped wear particles may entail changes in the resulting wear. This study focused with two approaches on the role of loose wear particles and their ejection in the wear of a fretted steel vs. steel contact in gross sliding conditions. In the first test series, loose wear debris was periodically removed from the interface and its effect on the wear was measured including multiple sliding amplitudes and two normal loads. In the second test series, the effect of specimen geometry on the resulting wear was studied.

EXPERIMENTAL

Apparatus design

A fretting apparatus based on an axisymmetrically loaded, annular, flat-on-flat, contact was used (Fig. 1A); described in detail elsewhere (Hintikka et al (14)). The contact occurred between two "tubular" specimens, one attached to a detachable specimen holder and the other to a fixed specimen holder with a conical clearance free fixture. The detachable specimen holder was attached to the end of the main shaft and the fixed specimen holder to the apparatus' frame with a steel plate. Contact was created by driving the fixed specimen holder and the steel plate in the *z*-direction with a hydraulic cylinder. The uniformity of the normal pressure was confirmed using a pressure sensitive film (Fuji prescale), and any error was corrected before the fretting test was started by adjusting the parallelism of the specimens (adjustments screws). Fretting movement was achieved by reciprocating rotational movement of the detachable specimen holder via the lever arm moved by an electric shaker. Measurements were run under controlled rotation amplitude using measured rotation as a feedback signal.

The *x*-, *y*-, *z*-displacements and rotation q between the two specimen holders were measured with 4 eddy current probes. Under ideal conditions, *x*- and *y*-displacements do not exist; however, changes in the interface will eventually result in uneven traction distribution causing such extra displacements. The total normal force P_{tot} was measured from the end of the piston rod with an s-beam load cell. The normal force at the specimens P was calculated as the total normal force minus the force required deforming the steel plate and the adjustment screws in the *z*-direction, which was separately calibrated. The frictional torque T was measured with strain gauges from the detachable specimen holder. Cyclic and static signals were measured at 5 kHz and 10 Hz frequencies, respectively.

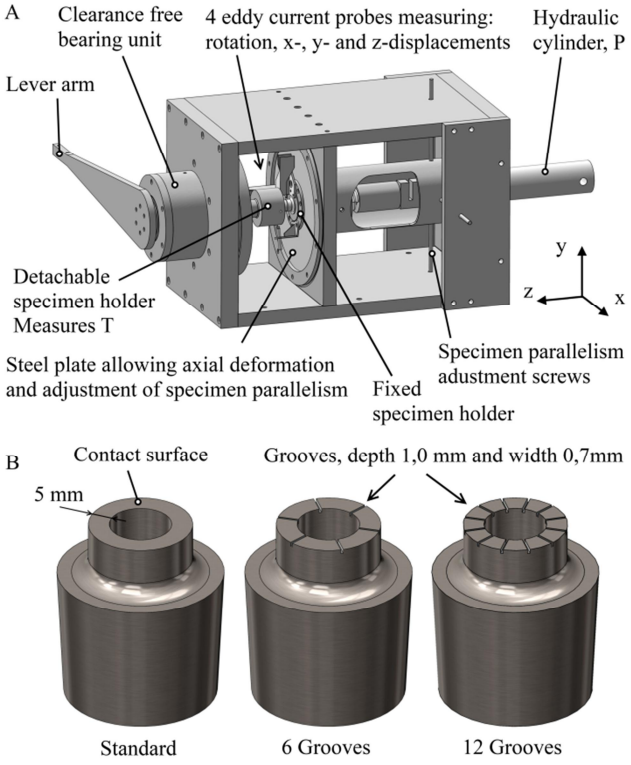

Figure 1 – Test rig and specimen design

Measured signals were recorded covering the entire experiment duration. One second long samples (40 cycles) were collected from the full duration data at exponentially increasing time intervals. The first five subsequent fretting load cycles were identified from each data sample, from which an average fretting loop was calculated. In the case of static signals, such as the normal load, the average value was calculated from the whole sample duration. The calculated average values were used in the further analysis.

Calculations

The rotation at the interface was calculated as the measured rotation q minus the shear deformation due to specimen compliance k (11.6×10^{-6} rad/Nm) under the frictional torque T as follows:

$$q_k = q - k \cdot T \quad (1)$$

The surface sliding was estimated using an average distance r_a of 10 mm as follows:

$$u = q_k \cdot r_a \quad (2)$$

Assuming that the COF is uniformly distributed, it can be calculated from the measured torque and the normal pressure distribution $p(r,\varphi)$ as follows:

$$COF_T = T / \left(\int_0^{2\pi} \int_{r_i}^{r_o} p(r,\varphi)\, dr\, d\varphi \right) \quad (3)$$

Each fretting cycle produces frictional work Ed due to frictional rubbing of surfaces. The COF was also calculated from the measured frictional energy dissipation Ed, the normal pressure distribution $p(r,\varphi)$ and the rotation amplitude q_a as follows:

$$COF_{Ed} = \frac{Ed}{4 \cdot q_a} / \left(\int_0^{2\pi} \int_{r_i}^{r_o} p(r,\varphi)\, dr\, d\varphi \right) \quad (4)$$

COF_{Ed} represents the average COF during one load cycle. In this study, COF_T was calculated using the amplitude of measured T, hence COF_T represent the maximum COF during one load cycle. In ideal conditions COF_{Ed} is equal to COF_T; however, under no called non-Coulomb friction conditions COF_T is greater than COF_{Ed} (Mulvihill et al (17), and Hintikka et al (14, 18, 19)).

Specimens

The specimens were made of a quenched and tempered steel rod (EN 10083-1-34CrNiMo6+QT, D 45 mm; design shown in Fig. 1B). Three kinds of specimens were used: standard annular specimens and ones with the contacting surface modified with 6 and 12 grooves. The specimens were turned to shape, and the annular contact surface was fine-ground so that the grinding scratches were circular. The grooves were made before the final fine-grinding of the contact surface. The material and surface roughness data is compiled in Table 1. Specimens were cleaned in an ultrasonic cleaning device with acetone before and after the fretting tests.

In tests with grooved specimens the nominal contact area was reduced by about 7 % and 13 % in the case of 6 and 12 grooves, respectively; hence the increase in the nominal surface pressure was quite low. Additionally, the contact between grooved and standard specimens introduced a local pressure concentration due to edge effects, leading to a further local increase in the surface normal pressure. The contact pressure distribution was estimated with the finite element method (Abaqus) using an approximately 100-µm element size. In ideal conditions, the local maximum pressure is infinite at the edge of the groove; however, it drops steeply close to nominal values. The impact of the actual, non-uniform surface pressure distribution on the calculated COF was estimated to deviate only about 1% compared to the contact of standard specimens (Eqs. 3 and 4). The FEM model did not accurately reproduce the peak surface pressure; however, its effect on the COF was negligible because the peak pressure was confined to a very small area. Hence all tests were analysed using a constant normal pressure approximation.

Furthermore, increased wearing may occur at the location of the normal pressure peaks. This leads to gradual change in the specimen geometry resulting in curved contact surfaces and change towards constant normal pressure conditions. Analytical solution for the geometry of a rigid punch against an elastic half-plane, producing constant normal pressure (Hills et al (2)), was compared to the sharp edged punch geometry. Using grooved specimen dimensions, the volume difference corresponded to wear masses of 0.7 mg and 0.3 mg for specimen with 6 and 12 grooves respectively. Hence, the wearing down of normal pressure peaks, near groove edges, cannot have a major impact on the resulting wear.

Table 1 – Specimen properties

S_y [MPa]	S_u [MPa]	E [GPa]	n
994	1075	210	0.27
S_a [µm]	S_q [µm]	S_z [µm]	
0.17 – 0.36	0.22 – 0.74	1.8 – 10.7	

Measurements

The experiment procedure was as follows. First, specimens were attached to the apparatus, specimen parallelism was confirmed, and the desired surface normal pressure was applied. Then the sliding amplitude was increased linearly within 400 load cycles from zero to the target level. The loading frequency was 40 Hz. The parallelism of the contacting surfaces was periodically adjusted by minimizing *x*- and *y*-displacements. Experiments were run in standard, monitored laboratory atmosphere (temperature 24˚C - 30˚C and humidity 7 % - 44 %).

A series of fretting tests were run by rubbing two standard specimens against each other for $3.0 \cdot 10^6$ load cycles at 10 MPa, 30 MPa, and 50 MPa nominal normal pressures and 5, 20, 35, 50, and 65-µm sliding amplitudes (reported in detail elsewhere by Hintikka et al (14)). A total of 19 tests were done, including reruns with identical test parameters, and these tests are named here as tests with standard specimens (Sta). Two new test series were performed: contact cleaning tests (Cle) and tests with grooved contact geometry (Gro). The wear results of the new test series were compared with those of the Sta tests.

In the contact cleaning tests (Cle), the contact was opened and cleaned after each $216 \cdot 10^3$ load cycles (90 min at 40 Hz) without removing the specimens from the apparatus. The test duration was $3.0 \cdot 10^6$ load cycles hence a total of 14 contact cleanings was done in each test. Contact cleaning was done as follows: first, the experiment was started as described above, and the contact was fretted for $216 \cdot 10^3$ load cycles. The contact was then opened by removing the normal force, and the interface was blasted with pressurized air, and the contact surfaces were rubbed with paper tissue soaked in acetone. This procedure removed a large proportion of loose wear debris from the interface. The design of the apparatus (no clearances) allowed opening and closing of the contact so that movement occurred only in the *z*-direction without disturbing the relative orientation (*x*, *y*) of the contacting surfaces. Experiments were made with a normal pressure of 10 MPa and 30 MPa and with various sliding amplitudes (7 tests).

In the Gro_6 and Gro_{12} tests, one standard specimen was fretted against one grooved specimen and the index refers to the number of grooves (Fig. 1B). Adding grooves to the interface may increase the probability of wear particle ejection because of the edges introduced perpendicular to the direction of the fretting movement. The grooves provide space for wear particles to accumulate, and their open ends allow the particles to trickle out. The test duration was $3.0 \cdot 10^6$ load cycles. Experiments were made with a normal force of 9425 N, corresponding to 30 MPa of normal pressure with standard specimens, and with various sliding amplitudes (6 tests). The normal force was chosen the same as that used in the Sta tests because Archard wear formalism predicts that the wear volume loss depends on the normal force rather than the surface pressure (Archard (20)). The test matrix is summarized in Table 2, where each row includes multiple experiments with different sliding amplitudes. Each test point was a separate measurement and was done using new specimens.

Table 2 – Test matrix

Series	P[N]	p_n [MPa]	u_a [µm]
Sta	3142	10	5, 20, 35, 50, 65
Sta	9425	30	5, 20, 35, 50, 65
Sta	15708	50	20, 35, 50
Cle	3142	10	20, 35, 50
Cle	9425	30	5, 20, 35, 50
Gro_6	9425	32.1	20, 35, 50
Gro_{12}	9425	34.6	20, 35, 50

Specimens were weighed prior and after tests with precision scales (Precisa EP 420A). Each specimen was warmed to 105˚C removing adhered moisture. Weighing was done three times with a reference weight and the average value was calculated. At each test point, mass loss was calculated as the sum of the mass losses of both specimens. The wear debris was analysed using X-ray diffractometer (Panalytical Empyrean), and the fretting scars were investigated using scanning electron microscope (SEM, Philips XL-30) and an energy dispersive X-ray spectroscopy (EDS, EDAX DX 4). Surface profiles were measured with a white light vertical scanning interferometer (Wyco NT1100). The surface roughness values of fretted surfaces were measured from

three different locations from each specimen. For each test point the average values were calculated covering both involved specimens. The dimensions of profiled areas were 3.8 mm × 4.6 mm, representing a total of 17 % of the combined contact area.

RESULTS

Friction coefficient

Fig. 2 shows fretting loops from all test series, which were extracted at 216×10^3 load cycles corresponding to the first contact cleaning in the Cle tests. Fig. 2A shows the last fretting loop before the experiment was halted for the first contact cleaning with a solid black line. After the contact cleaning, the fretting loop gradually develops as the rotation amplitude approaches its target value during the mid-experiment start-up phase (dashed grey lines), and then stabilizes to nearly identical shape what existed prior contact cleaning (dashed black line). Fig. 2B, 2C and 2D compares fretting loops from Cle, Gro_6 and Gro_{12} test series against the Sta tests, illustrating that the fretting loop shapes were nearly identical.

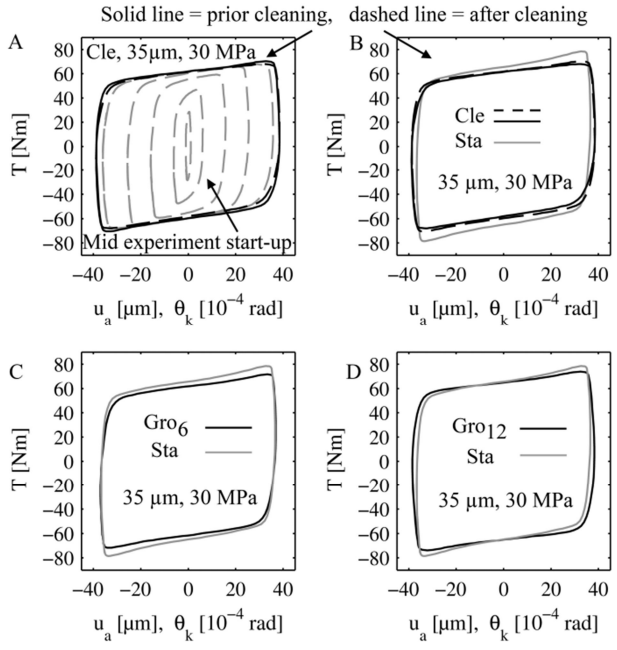

Figure 2 – Fretting loops after 216×10^3 load cycles

The overall frictional behaviour, including values of COFs and shapes of fretting loops, related to the Sta tests was described in detail elsewhere (Hintikka et al (14)). In standard tests, the COF_T was observed as initially high, in the range of 1.2 to 1.5, followed by a sharp drop to steady state values in the range of 0.6 to 0.8. The COF_{Ed} showed similar behaviour, though its maximum value was in the range of 0.9 to 1.1 and dropped to 0.6 - 0.7 in steady state conditions. Additionally, the initial high COF conditions were characterized by non-Coulomb friction conditions, where the COF value depended on the specimens' rotational position during a fretting cycle (Fig. 2). In non-Coulomb conditions, $COF_T > COF_{Ed}$, as can be seen in the COF graphs in Fig. 3.

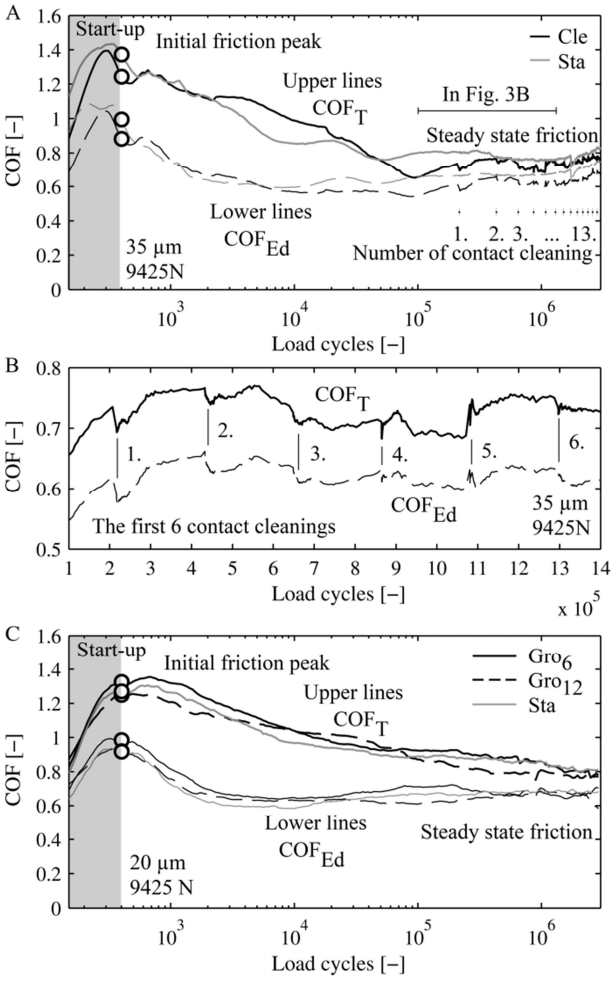

Figure 3 – COF in Cle tests (A&B) and Gro_6 and Gro_{12} tests (C)

Fig. 3A compares friction results between Sta and Cle tests. After the first start-up, frictional behaviour was nearly identical between the two, which is obvious because the test conditions were identical. Subsequent start-ups after each cleaning produced no extra peaking in the COF, its value remaining mostly unaffected by contact cleaning, which stabilized at about its steady state value. However, there were small abrupt changes in the COFs due to the cleaning, which is illustrated in greater detail in Fig. 3B showing the first six contact cleanings. It may be that after each mid-experiment cleaning enough loose wear debris and hard to-remove third body screens remained in the interface to maintain steady state friction conditions. The mid-experiment start-up phases were excluded from this graph. Similarly the Gro tests produced a COF nearly identical to that observed in the Sta

tests which is illustrated in Fig. 3C.

It follows from the friction results that any difference in the entrapped third body particles, between the three test series, caused no marked differences in the fretting loop shapes or in the values of COF_T or COF_{Ed}. Therefore, any differences in the wear results, which are shown next, cannot be explained by changes in frictional behaviour because it remained unchanged.

Fretting wear

The mass losses of Cle tests are compared against Sta test in Fig. 4. First, Sta tests produced wear mass loss mostly dependent on the accumulated sliding distance or sliding amplitude, whereas the normal load had only a low impact on it. Compared to the Sta tests, Cle tests produced three to four times greater mass losses at 3142 N and 9425 N normal loads (Fig. 4A). In them, mass loss depended mostly on the accumulated sliding distance, and normal load had only a minimal effect.

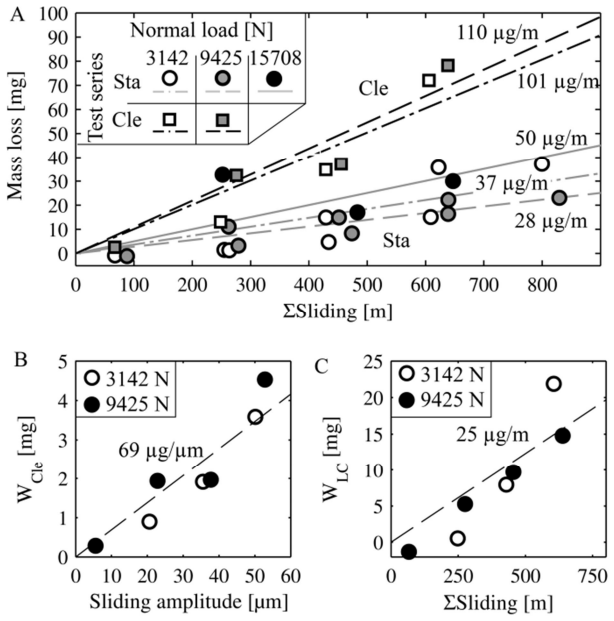

Figure 4 - Mass loss due to fretting wear in Cle tests

Each test point in the Cle tests was subjected to a total of 13 cleanings during the test and once after the test, whereas in Sta tests they were cleaned once after the test. It follows that the number of contact cleanings (N_{Cle}) was 1 and 14 for Sta and Cle test series, respectively. The contribution of each cleaning on the wear mass was approximated by assuming that the total wear mass (W_{tot}) is the combination of gradual wear due to load cycles and sliding amplitude (W_{LC}) and the sum of the masses due to cleaning (W_{Cle}), as shown in Eq. 5.

$$W_{tot} = W_{LC} + N_{Cle} \acute{} \; W_{Cle} \tag{5}$$

The calculated values for W_{LC} and W_{Cle} are shown in Fig. 4B and 4C. The wear due to load cycles (W_{LC}) and each contact cleaning (W_{Cle}) were approximately linearly dependent on the sliding amplitude and accumulated sliding distance, respectively, and those were independent of the normal load. Hence the wear enhancing effect of cleanings increased as a function of the sliding amplitude.

In annular flat-on-flat contact, wear particles may be ejected naturally only from the inner and outer edges of the contact. This however requires that the wear particles migrates perpendicular to the fretting direction. The grooved specimens introduced additional edges, from which the wear particles may be ejected after migrating parallel to the fretting. Wear results from Gro_6 and Gro_{12} tests are compiled in Fig. 5, showing that using grooved specimens increases wear significantly. Wear increased approximately linearly as a function of the accumulated sliding distance. Furthermore, wearing was greater with 12 grooves than with 6 grooves. The wear increasing effect of the grooves is clearly illustrated in Fig. 5B, showing the measured wear rates from Sta, Gro_6 and Gro_{12} tests. The wear rate was calculated as mass loss divided by the accumulated sliding distance. The observed increase in the wear cannot be explained by the local pressure peaks near to the groove edges, because rounding of the interface may explain only about 1 mg mass loss, which is insignificant in comparison to the measured wear mass losses. Furthermore, the grooves changed the nominal contact area and nominal contact pressure only by a small amount (~10%).

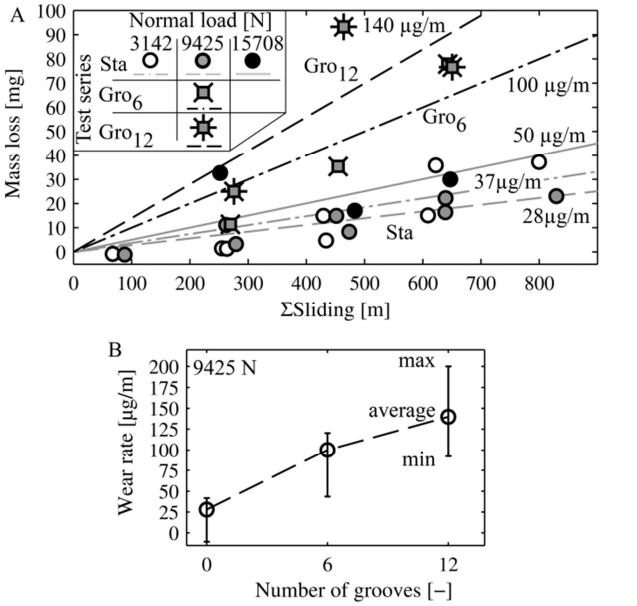

Figure 5 - Mass loss due to fretting wear in Gro_6 and Gro_{12} tests

The ejected wear debris was analysed using x-ray diffractometer covering the Gro tests and some of the Sta tests. Wear debris was composed of hematite (α-Fe_2O_3) and trace amounts of iron (steel particles). This result is typical for fretted steel contacts (Waterhouse (1)).

Fretting scars

A compilation of SEM micrographs and EDS results, including samples from all test series, is shown in Fig.6. The elemental composition of the fretting scar surface was mostly iron with small amount of alloying elements corresponding to quenched and tempered steel, with varying amounts of oxygen. Therefore, only the percentage of oxygen atoms (*At-%*) is shown, indicating the level of oxidation.

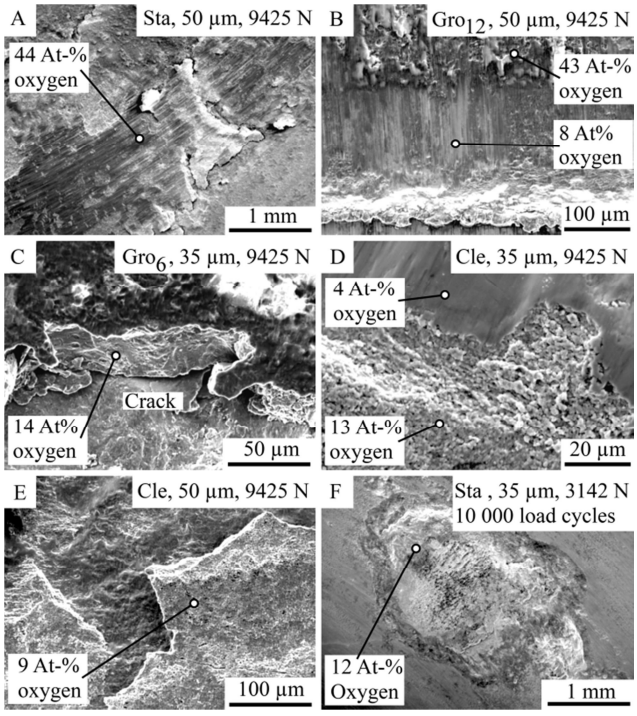

Figure 6 – Fretting scar micrographs (SEM and EDS)

The specimen surfaces were covered with a layer of oxide wear particles as shown in Fig. 6A. The oxygen content was approximately 40 *At-%* indicating a high level of oxidation. It may be that the oxide layer is composed of agglomerated hematite, or other iron oxides, and steel particles. Basically, this kind of oxide layer was found in all tests, and represents a typical fretted surface in this study.

Fig. 6B shows an example of the wear track on a standard specimen which was fretted with a grooved specimen. It was observed that section of surface, related to the location of the groove edge, was mostly clean of oxides (8 *At-%*); however regions further away from the groove edge were covered in oxides, comparable to other test series (43 *At-%*). Interestingly the width of the clean area is approximately twice the sliding amplitude (100 µm). This demonstrates that oxides are removed efficiently at the edge perpendicular to the fretting direction. Fig. 6C shows an example of cracking in the specimen surface and spot from which metal particle had detached. Detachment of metallic particles due to surface fatigue is one source of fresh wear particles. Mostly metallic, compacted wear debris was observed as shown in Fig. 6D and 6F. Such layers were composed of, approximately 1 µm sized, mostly metallic steel particles which had agglomerated, indicating that fresh wear particles were generated at this site. Metallic wear debris agglomerates were found from most specimens, typically in a form of few spots which sizes varied from few to few tens of square millimetres. It is likely that these kinds of metal agglomerates gradually changed to highly oxidized layers.

In a previous study adhesive wear resulting in material transfer was reported to occur during the first few thousands of load cycles (Hintikka et al (14,19)). An example of material transfer layer is shown in Fig. 6E. The initial material transfer lead to tangential fretting scar interlocking and it had a profound effect on the COF (Hintikka et al (19)). There was no evidence of further material transfer after the first few thousands of load cycles; however the initial adhesive wear followed by gradual wearing down of metallic transfer layers is part of the fretting wear phenomenon.

Examples of the measured surface profiles from Gro_6 and Gro_{12} tests are shown in Fig. 7. Some surface profiles showed gentle curvature near grooves which may have been caused by the initial normal pressure distribution which is illustrated in Fig. 7A (Gro_6, 35 µm, 9425 N). However the wear track profile is characterized by protrusions and depressions introducing extra normal pressure peaks. The wear tracks illustrated frequently wearing which clearly did not follow the shape of a constant normal pressure distribution as illustrated in Fig. 7B (Gro_{12}, 50 µm and 9425 N). Though some rounding of the groove edges occurred, it did not have significant contribution to the overall wear and it did not occur systematically. The specimens did not wear under the grooves, resulting in strips of nearly intact surfaces. Theoretical wear depths (dashed lines), calculated using the measured weight loss, specimen nominal contact area and steel density, shows close match to measured wear depth. This also verifies that the mass losses were measured with good accuracy.

Fretting increased the specimen surface roughness and the resulting S_a was dependent on the test series, normal load and sliding amplitude as shown in Fig. 8A. Typically the S_a increased as a function of sliding amplitude and normal load in all test series. Additionally, S_a was lower in Sta tests than in Gro or Cle tests, which can be attributed partly to lower

wear mass loss in the Sta tests.

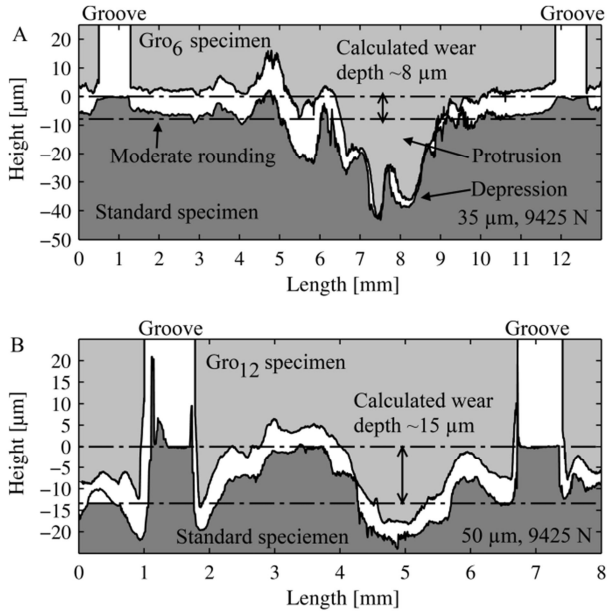

Figure 7 - Wear scar profiles in Gro_6 and Gro_{12} tests

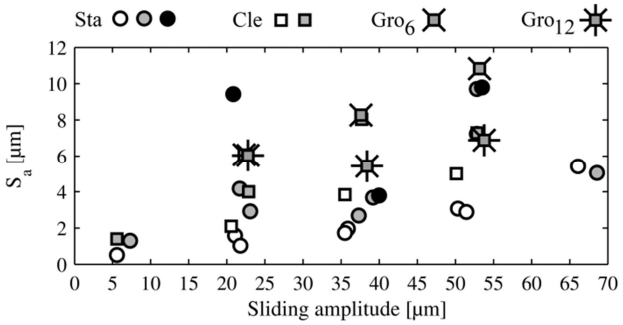

Figure 8 – Surface roughness after fretting tests

DISCUSSION

Experiments showed that oxide wear particles (hematite) were entrapped and ejected from the interface. Additionally, the specimens were covered in hard to remove iron oxide and metallic particle agglomerates. The wear results of this study are conveniently explained by the velocity accommodation in the third bodies, which is known to be pronounced in fretting conditions. The idea being that the first bodies are separated by third body screens and third body bulk in the middle. The fretting movement between first bodies is accommodated, at least partly in the third bodies providing protection against wear.

The Cle tests illustrated that removal of entrapped wear debris lead to significant increase in wear, and that the effect increased linearly as a function of sliding amplitude, while normal load had unobservable effect on it. In the scheme of velocity accommodation, the cleaning removed much of the third body bulk, resulting temporary increase in wear rate. The thickness of the third body bulk would then increase due to the entrapment of wear particles and wear rate would gradually recover back to lower values. Although this explains the increased wear in comparison to the Sta test, it does not explain why the wear increasing effect was depended on the sliding amplitude. A possible explanation would be that the amount of entrapped wear debris, which was removed in each cleaning, increased as a function of sliding amplitude. In such conditions Fig. 4B may also represent the amount of entrapped wear debris which was removed in each leaning. Such behaviour may be explained by the velocity accommodation scheme, assuming that the greater the sliding amplitude the thicker the third body bulk needs to be, before a certain level of wear reduction is achieved.

The same mechanism may be also used to explain the wear results from the Gro tests. The reciprocating shearing of wear particles in the interface provided some velocity accommodation. This shearing occurred in the fretting direction, though there may be some randomness in the movement of individual wear particles due to interactions between other wear particles and the specimens' surfaces. This enables migration of wear particles which is suspected to occur mostly in the fretting direction; however it may occur in any direction. A wear particle may only be ejected when it is at a free edge. It follows that ejection of wear particles occurs more frequently at the edges perpendicular to fretting direction. Additionally, it was observed that area next to the groove edge was relatively clean from oxides. The width of this 'clean' area was approximately twice as large as the sliding amplitude, which may imply that the edge of the groove scraped off entrapped adhering third bodies, potentially increasing the ejection rate. Overall, the introduction of grooves increased wear particle ejection rate, reducing the thickness of the third body bulk and the wear protection it offers, leading to an overall increase in wear. Because all test series showed approximately linear dependency between mass loss and sliding amplitude it is suspected that the flowing of wear particles towards parallel and perpendicular edges was mostly dependent on the sliding amplitude. In cylinder against flat contact configuration wear rate reduced when the contact width was increased, while the contact length remained at a constant value, suggesting that the contact size itself plays a role (Warmuth et al (13)). In this study the grooves were equally spaced thus increasing the number of grooves reduced the distance between grooves. The average distance which a wear particle needs to migrate before encountering a contact edge is dependent on this distance, suggesting that the contact size effect on fretting wear is dependent on the distance between contact edges in the fretting direction.

The wear mass loss was mostly independent of the normal load in both the Sta and Cle tests contradicting classic

Archard theory (Archard (20)). In steady state velocity accommodation conditions the wear depends on the wear particle ejection. Increasing the rate of contact cleanings and or the number of grooves might bring about the expected normal load dependency. Additionally, direct observations of the thickness of the third body bulk, under fretting conditions, might shed more light on the velocity accommodation mechanics. Such experimental investigation is left for future study.

CONCLUSIONS

Gross sliding fretting wear tests were run with annular, flat-on-flat contact, using quenched and tempered steel specimens. The effect of loose wear particles on wear rate was studied by running tests in which loose wear particles were periodically removed from the interface; in addition, tests were run with grooved contact surfaces. The following conclusions were drawn:

1. The fretting loop shapes and values of the average and the maximum coefficient of friction remained unaffected by the contact cleaning and by the use of grooved specimen geometry.
2. Loose wear particles in the interface protect against wear. Removing them from the interface increased wear rate significantly. This effect increased approximately linearly as a function of the sliding amplitude. Normal load had no marked effect on wear in the test conditions.
3. Specimen geometry had a strong effect on wear rate because grooves perpendicular to the sliding motion increased wear rate. The wear promoting effect of the grooves increased when the number of grooves was increased.

ACNOWLEDGEMENTS

This study was conducted as part of the SCarFace research project. We are grateful for the financial support provided by Tekes (Finnish Funding Agency for Technology and Innovation, decision number 40205/12), Wärtsilä Finland Oy, Nome Oy, and Global Boiler Works Oy. The authors give their thanks to MSc. Ville Oksanen for providing SEM images and EDS data and MSc. Leo Hyvärinen for the X-ray diffractometry measurements.

REFERENCES

(1) Waterhouse R.B. (1972),"Fretting corrosion," Pergamon press, Oxford, ISBN 0 08 16902 3

(2) Hills D.A Nowell D (1994), "Mechanics of fretting fatigue," Kluwer Academic Publishers, Dordrecht, ISBN 0-7923-2866-3.

(3) Berthier, Y., Godet, M., Brendle, M. (1989), "Velocity accommodation in friction." *Tribology Trasactions*, 32, pp 490.

(4) Berthier, Y. (1990), "Experimental evidence for friction and wear modelling," *Wear*, **139**, pp 77-92.

(5) Godet, M. (1984), "The third-body approach: A mechanical view of wear," *Wear*, **100**, pp 437-452.

(6) Godet, M. (1990), "Third-bodies in tribology," *Wear*, **136**, pp 29-45.

(7) Berthier, Y., Vincent, L., Godet, M. (1988), "Velocity accommodation in fretting," *Wear*, **125**, pp 25-38.

(8) Iordanoff, I., Berthier, Y., Descartes, S., Heshmat, H. (2002), "A Review of Recent Approaches for Modeling Solid Third Bodies," *Journal of Tribology*, **124**, pp 725-735.

(9) Heshmat, H. (1991), "The Rheology and Hydrodynamics of Dry Powder Lubrication," *Tribology Transactions*, **34**, pp 433-439.

(10) Haff, P.K. (1983), "Grain flow as a fluid-mechanical phenomenon," *Journal of Fluid Mechanics*, **134**, pp 401-430.

(11) Colombié, C., Berthier, Y., Floquet, A., Vincent, L., Godet, M. (1984), "Fretting: Load Carrying Capacity of Wear Debris," *Journal of Tribology*, **106**, pp 194-201.

(12) Merhej, R., Fouvry, S. (2009), "Contact size effect on fretting wear behaviour: application to an AISI 52100/AISI 52100 interface," *Lubrication Science*, **21**, pp 83-102.

(13) Warmuth, A.R., Pearson, S.R., Shipway, P.H., Sun, W. (2013), "The effect of contact geometry on fretting wear rates and mechanisms for a high strength steel," *Wear*, **301**, pp 491-500.

(14) Hintikka, J., Lehtovaara, A., Mäntylä, A. (2014), "Fretting-induced friction and wear in large flat-on-flat contact with quenched and tempered steel," *Tribology International*, **92**, pp. 191–202.

(15) Varenberg, M., Halperin, G., Etsion, I. (2002), "Different aspects of the role of wear debris in fretting wear," *Wear*, **252**, pp 902-910.

(16) Blau, P.J. (2015), "How common is the steady-state? The implications of wear transitions for materials selection and design," *Wear*, **332-333**, pp. 1120-1128.

(17) Mulvihill, D.M., Kartal, M.E., Olver, A.V., Nowell, D., Hills, D.A. (2011), "Investigation of non-Coulomb friction behaviour in reciprocating sliding," *Wear*, **271**, pp 802-816.

(18) Hintikka, J., Lehtovaara, A., Mäntylä, A. (2014), "Non-Coulomb friction in gross sliding fretting conditions with aluminium bronze against quenched and tempered steel," *Tribology International*, **79**, pp 151-161.

(19) Hintikka, J., Lehtovaara, A., Mäntylä, A. (2016), "Normal displacements in non-Coulomb friction conditions during fretting," *Tribology International*, **94**, pp. 633–639.

(20) Archard, J.F. (1953), "Contact and Rubbing of Flat Surfaces," *Journal of Applied Physics*, **24**, pp 981-988.